Title
Freeze-Dried Sulfur–Graphene Oxide–Carbon Nanotube Nanocomposite for High Sulfur-Loading Lithium/Sulfur Cells

Journal
Nano Letters, 17(11)

ISSN
1530-6984

Authors
Hwa, Yoon
Seo, Hyeon Kook
Yuk, Jong-min
et al.

Publication Date
2017-11-08

DOI
10.1021/acs.nanolett.7b03831

Peer reviewed

Freeze-Dried Sulfur-Graphene Oxide-Carbon Nanotube Nano-composite for High Sulfur Loading Lithium/Sulfur Cells

*Yoon Hwa,[1,2] Hyeon Kook Seo,[3] Jong-min Yuk[3] and Elton J. Cairns[1,2,]**

1 Energy Storage and Distributed Resources Division, Lawrence Berkeley National Laboratory Berkeley, California, 94720, USA

2 Department of Chemical and Biomolecular Engineering University of California, Berkeley, California, 94720, USA

3 Department of Materials Science and Engineering, Korea Advanced Institute of Science and Technology, Daejeon, 34141, Republic of Korea

KEYWORDS. Lithium sulfur cell, Energy storage, High sulfur loading, Aluminum foam, Ionic liquid, In situ TEM

ABSTRACT.

The ambient-temperature rechargeable lithium/sulfur (Li/S) cell is a strong candidate for the beyond lithium ion cell, since significant progress on developing advanced sulfur electrodes with high sulfur loading has been made. Here we report on a new sulfur electrode active material consisting of a cetyltrimethylammonium bromide-modified sulfur-graphene oxide-carbon nanotube (S-GO-CTA-CNT) nano-composite prepared by freeze drying. We show the real-time formation of nano-crystalline lithium sulfide (Li_2S) at the interface between the S-GO-CTA-CNT nano-composite and the liquid electrolyte by *in situ* TEM observation of the reaction. The combination of GO and CNT helps to maintain the structural integrity of the S-GO-CTA-CNT nano-composite during lithiation/delithiation. A high S loading (11.1 mgS/cm^2, 75 %S) S-GO-CTA-CNT electrode was successfully prepared using a 3-D structured Al foam as a substrate and showed good S utilization (1128 mAh/gS corresponding to 12.5 mAh/cm^2), even with a very low sulfur to electrolyte weight ratio of 4. Moreover, it was demonstrated that the ionic liquid in the electrolyte improves the Coulombic efficiency and stabilizes the morphology of the Li metal anode.

Main Text

In recent decades rechargeable batteries have been greatly influential on human life, where the synergies between rechargeable batteries and communication technologies led electronics into a wireless era. As the capability of rechargeable batteries to deliver high energy and power has advanced, their applications have expanded from small portable electronics to clean-powered transportation systems such as full electrical vehicles (EV) or aircraft. For long-range EVs, a specific energy of at least 300 Wh/kg with reasonable cost is desired, which is unfortunately beyond the practical limits of conventional Li ion batteries. For this reason, extensive research effort has been invested in developing beyond Li ion batteries that are capable of delivering very high specific energy.

The ambient temperature lithium/sulfur (Li/S) cell is one of the most promising alternatives because of its high theoretical specific energy of 2680 Wh/kg that is made possible by the large specific capacity of the S electrode (1675 mAh/gS *vs*. 272 mAh/g for a $LiCoO_2$ electrode) provided by the reaction:

$16Li^+ + S_8 + 16e^- \rightarrow Li_2S$ (E^0= 2.15 V)

Despite the great potential of the Li/S cell for high specific energy applications, it did not attract much interest in the battery community earlier, due to the drawbacks of the S electrode such as the poor electrical conductivity of S and Li_2S, the volume change of S particles, polysulfides dissolution into liquid organic electrolytes and the polysulfide shuttle phenomenon[1] that restrict the electrochemical utilization of S and its reversibility.

In recent years, significant progress on overcoming the drawbacks of the S electrode has been made by the rational design of S-based active materials[2-14] at the lab scale, showing excellent electrochemical performance. However, in spite of the progress on the S electrode, transferring the lab-scale technologies to industry for developing a practical high specific energy Li/S cell is still a significant challenge, mainly due to the low level of S loading (generally ~ 1.0 mgS/cm^2) and the high percentage 'dead weight' in the cells. Although higher S loading electrodes over 5.0 mgS/cm^2 have recently been reported,[15-29] only limited effort has been made to reduce the dead weight of the cells, which limits the obtainable specific energy. Therefore, intensive effort is necessary to reduce the dead weight for the Li/S cell in order to make it commercially attractive. Among the cell components contributing to the dead weight, the electrolyte is very influential because it is an essential component for electrochemical operation, which means that reducing the electrolyte amount must be done thoughtfully. The design calculations (Figure S1) clearly show that there is a significant opportunity for reaching 300 Wh/kg and more, when the S loading is 6 mg/cm^2 or higher with an electrolyte to sulfur weight ratio (E/S ratio) of less than 3.

Results and Discussion

In this work, the S-GO-CTA nano-composite reported in our previous work[3] was further modified by embedding CNTs between the S-GO-CTA flakes to improve the electronic conductivity of the S-GO-CTA nano-composite by acting as the electronic conduction pathway across the S-GO-CTA-CNT nano-composite. The synthesized S-GO-CTA-CNT nano-composite contained 87 % (*w/w*) of S which was confirmed by thermogravimetric analysis (TGA, Figure S2). The morphology of the S-GO-CTA-CNT composed of the thin GO flake-like particles with embedded CNTs without any significant agglomeration of S, even with the high S content of 87

%. The uniform distributions of S, C, O and N on the flake-like particles were shown by scanning electron microscopy (SEM, Figure 1a) and transmission electron microscopy (TEM, Figure 1b) with energy dispersive spectroscopy (EDS) elemental mapping. N is associated with the mixture of compounds derived from CTA. According to the X-ray photoelectron spectroscopy (XPS) results, both samples (with and without CTA) showed peaks that correspond to the S $2p_{3/2}$ and S $2p_{1/2}$,[30] however, only the S-GO-CNT nano-composite showed two more peaks near 168.4 and 170.5 eV which are associated with oxidized (by air) sulfur (sulfate species),[31] whereas that of the S-GO-CTA-CNT nano-composite did not show any peaks near 168~170 eV. Considering that XPS analysis is a surface sensitive technique, it is suggested that the mixture of compounds derived from CTA covers the S layer coated on the GO surface, so it may impede the surface oxidation of S or the oxidized S may be covered by a mixture of CTA-derived compounds, resulting in no XPS peaks near 168~170 eV. In the X-ray diffraction pattern (XRD, Figure 1d), all sharp peaks correspond to the α-S phase (JCPDS #08-2047). Based on the characterization results discussed above, the structure of the S-GO-CTA-CNT nano-composite is suggested as illustrated in Figure 1e, showing the mixture layer of the compounds derived from CTA, the α-S and the GO flakes, layer by layer. The S-GO-CTA-CNT electrode showed a better defined second discharge plateau than that of the S-GO-CTA electrode, which is attributed to the insertion of CNTs into the S-GO-CTA flakes (Figure S3).

Homogeneous Li_2S formation on the S electrode during the discharge process is one of the key issues for good electrochemical performance (due to the electrically insulating nature of Li_2S) since a thick accumulation of Li_2S can impede the electrochemical reaction of the remaining S. Therefore investigation into the reaction mechanism of S with Li ions is worthwhile for

understanding the structural benefit of the S-GO-CTA-CNT nano-composite. Since an organic liquid electrolyte is used in most Li/S cells, a real-time observation technique with the presence of a liquid electrolyte is appropriate for understanding the lithiation behavior of the S-GO-CTA-CNT nano-composite close to the conditions in the electrochemical cell. This has been an enormous challenge for studying Li-S cell reactions with the TEM.[32-34] The graphene liquid cell (GLC)-TEM technique is suitable, because S can be examined in the presence of the actual electrolyte in the GLC under the TEM, allowing the observation of the real-time reaction between S and Li ions occurring at the solid-liquid interface.[35-37] The GLCs were prepared by sealing S-GO-CTA-CNT nano-composites and electrolyte (EL) solution composed of 1 M Lithium bis(trifluoromethanesulfonyl)imide (LiTFSI) in 1,2-dioxolane (DOL)/1,3-dimethoxyethane (DME) (1:1, *v/v*)) together with two graphene sheets. As shown in Figure 2a, the Li ions from the LiTFSI in the electrolyte can be reduced by taking up electrons from the electron beam irradiation, so the chemical lithiation process of S in the GLCs can occur.[36-37]

As a result of time-series scanning TEM (STEM) shown in Figure 2b, the nucleation and growth of the Li_2S nano-crystals on the GO sheet was demonstrated which corresponds to the result of *in situ* atomic force microscopy.[38] After 132 s, very small (a few to 30 nm diameter) bright phases appeared and then they gradually grew or merged with newly appearing bright phases. Selected area-electron diffraction patterns (SA-EDPs) shown in Figure 2c confirm that the new phase is crystalline Li_2S. LiF was also detected in SA-EDPs which could be attributed to the election beam-assisted dissociation of LiTFSI in the electrolyte. Figure 2d graphically displays the growth of the Li_2S crystals on a 200×200 nm area with time. The nucleation of Li_2S particles with about 10 nm size was observed after 118 s and the nucleated nano-Li_2S grew alone

or coalesced up to 90 nm after 228 s rather than forming a big aggregation of Li_2S. In addition, the size and position of the hole on S-GO-CTA-CNT flake (black color) shown in Figure 2b did not significantly change during lithiation of S, which may indicate that the volume change of the S layer around the hole was not significant after forming the Li_2S. The results suggest that the nano-architecture of the S-GO-CTA-CNT composite leads to the homogeneous formation of Li_2S nano-crystals and helps to maintain its structural integrity during lithiation, which is a significant benefit for obtaining high S utilization and good cycling performance of the cell.

To electrochemically evaluate the prepared S-GO-CTA-CNT nano-composite, electrodes were prepared with a very porous 3D structured Al foam current collector (Figure S4). The 3D structured current collector is suitable for developing the high S loading electrode because the conductive framework with many pores can accommodate a large amount of the active S particles and the S particles can be supplied with both electrons and Li ions. Because of the benefits of the foam structure, it is easier to increase S content by reducing the amount of binder and carbon additives without sacrificing cell performance. As shown in Figure S5a, the Al foam electrode showed a high specific capacity of between 900 ~ 1000 mAh/gS for 80 cycles, while the Al foil electrode delivered a specific discharge capacity of only about 150 mAh/gS at 0.8 mA/cm^2 (average S loading: 3.1 mg/cm^2, 70 %S). The voltage profiles of the Al foam and Al foil electrodes (Figure S5b) are significantly different, wherein the Al foam electrode showed typical discharge voltage profiles, showing two plateaus at between 2.4 ~ 2.1 V (*vs*. Li/Li^+), which are associated with the formation of high-order polysulfides (Li_2S_n, $n \geq 4$) and low-order polysulfides (Li_2S_n, $n < 4$) and insoluble Li_2S, respectively. In contrast, the Al foil electrode did not exhibit the second discharge plateau at 0.8 mA/cm^2, resulting in the poor S utilization. The

Nyquist plots of the Al foam electrode obtained at the charged state (Figure S5c) showed a lower cell impedance for both the electrochemical reaction (the semicircle in the middle frequency region) and mass transport (the sloping line in the low frequency region) than that of the Al foil electrode, indicating that the Al foam electrode provides better conditions for the electrochemical process, e.g. porous structure or large surface area for the electrochemical reaction.

For the high S loading electrode (11.5 mgS/cm^2), the large amount of electrode material was successfully accommodated in the Al foam substrate as shown in Figure S6. The high S loading electrode showed the characteristic discharge voltage profiles of the Li/S cell with a high specific capacity of 900-1178 mAh/gS (corresponding to 10-13.6 mAh/cm^2) for 10 cycles (Figure 3a and 3b). The long term cyclability of the electrode (2.3 mgS/cm^2, 70 %S) was also demonstrated for 300 cycles at 0.2 and 1.0 mA/cm^2 for the first and following cycles, respectively. The two distinguishable discharge plateaus could still be obtained at the higher current density of 1.0 mA/cm^2 with the initial specific discharge capacity of 1141 mAh/gS (Figure 3c). During long-term cycling (Figure 3d), the electrode delivered a specific discharge capacity 827 and 557 mAh/gS at the second and 300th cycles, respectively, at 1.0 mA/cm^2. With the higher S loadings of 4.2 mg/cm^2 and 7.9 mg/cm^2, the electrodes still showed good cyclability for 100 cycles (0.2 mA/cm^2 for the first cycles and 0.4 mA/cm^2 for the following cycles, volume fraction of ionic liquid in the electrolyte: 33.3 %, Figure 3e) and 40 cycles (0.2 mA/cm^2 for the first 10 cycles and 0.4 mA/cm^2 for the following cycles, volume fraction of ionic liquid in the electrolyte: 0.20, Figure 3f), respectively. After 100 cycles, the S-GO-CTA-CNT nano-composite maintained its unique nano-architecture without aggregation of S, as shown in the SEM image of the cycled S-GO-CTA-CNT nano-composite (Figure S7).

Since the supply of electrons and Li ions to the active S particles becomes very important for maintaining the electrochemical performance of the cells, as the S loading and S content increase, it is worthwhile to further modify the S-GO-CTA-CNT nano-composite. Although the S-GO-CTA-CNT nano-composite has a homogenous flake-like morphology, aggregation of the flakes could not be avoided due to the strong aggregation tendency of GO after conventional vacuum filtration and drying processes, which may cause isolation of some deposited S on the GO flakes from the electrochemical reaction. To obtain a thinner and unaggregated structure of the S-GO-CTA-CNT nano-composite, the freeze-drying method was evaluated, which can suppress the aggregation of GO flakes by using the volume expansion of H_2O that occurs during freezing. The volume that was occupied by the ice remains empty space when the ice is sublimed. As a result of freeze drying for the S-GO-CTA-CNT nano-composite (S-GO-CTA-CNT (FD)), ultra-thin S-GO-CTA-CNT flakes which seem to be only a few layers thick were obtained (Figure 4a, low magnification images of the S-GO-CTA-CNT and S-GO-CTA-CNT (FD) are shown in Figure S8). The EDS elemental mapping results (conducted for the marked area) and TGA results (Figure S9, 86 %) confirmed that the freeze-drying process does not influence the distribution of the elements and the S content of the S-GO-CTA-CNT nano-composite.

The evaluation result for the S-GO-CTA-CNT (FD) electrode (6.3 mgS/cm^2, 75 %S) showed significantly better electrochemical behavior than that of the S-GO-CTA-CNT electrode, showing a high discharge specific capacity of 1200 mAh/gS (*vs*. 1117 mAh/gS for the S-GO-CTA-CNT electrode) and lower overpotentials (Figure 4b). The cycling performance of the S-GO-CTA-CNT (FD) electrode was also improved with a discharge capacity retention of about 82

% after 10 cycles, while that of the S-GO-CTA-CNT electrode was 76 % (Figure 4c). This improvement can be attributed to the open structure of the S-GO-CTA-CNT (FD) nano-composite that allows more S to be involved in the electrochemical reaction, which is supported by the EIS results (Figure S10), exhibiting lower cell impedance in both aspects of electrochemical reaction rate and mass transport compared to that of the S-GO-CTA-CNT electrode. To enhance the obtainable specific energy of the cells, the E/S ratio was reduced from 10 to 5 and the S-GO-CTA-CNT (FD) electrode was still capable of delivering high specific discharge capacity of up to 1200 mAh/gS at 0.2 mA/cm^2, even as the E/S ratio was reduced to 5. At the E/S ratio of 5, although the specific capacity of the electrode was little decreased compared to that obtained with an E/S ratio of 10 (1357 mAh/gS), the operating voltages of the cells was almost the same, which is also important for high specific energy (Figure S11a). Both the cells with E/S ratios of 10 and 5 showed good cycling performance with specific discharge capacities of 1020 and 923 mAh/gS, respectively, after 12 cycles (Figure S11b). The rate performance of the cell with the E/S ratio of 5 was investigated and it showed typical discharge voltage profiles with the specific capacity of 1265-955 mA/cm^2 at 0.2-1.2 mA/cm^2 (Figure 4d) from the first to sixth cycle and stable cycling for the following cycles at 1.2 mA/cm^2 (Figure 4e).

The further reduced E/S ratio of 4 that is very close to the desired target of 3 was also explored with the S-GO-CTA-CNT (FD) electrode (S loading: 11.1 mgS/cm^2, 75 %S) and a high specific discharge capacity of 1128 mAh/gS was obtained (corresponding to 12.5 mAh/cm^2) for the first discharge (Figure S12). The E/S ratio of 4 represents significant progress among the high S loading electrode works which are listed in Table S1, and is the lowest E/S ratio reported so far.

As a result, the high specific energy of 332 Wh/kg (excluding the weight of cell housing, assuming a 2 electrodes cell) can be achieved according to the design calculations.

To investigate the effect of ionic liquid ($PYR_{14}TFSI$) on the electrochemical behavior of the high S loading cells (6.3 mgS/cm^2, 75 % S), the electrochemical test results obtained using the ionic liquid-containing electrolyte (1 M LiTFSI + 0.5 M $LiNO_3$ dissolved in $PYR_{14}TFSI$:DOL:DME=1:1:1, *v/v*) and the conventional electrolyte (1 M LiTFSI + 0.5 M $LiNO_3$ dissolved in DOL:DME=1:1, *v/v*) are compared in Figure 5a and 5b. It is known that the ionic liquid existing in the electrolyte plays an important role, not only to limit the polysulfide dissolution and their shuttle to the Li electrode,[39-40] but also to stabilize the Li electrode during cycling.[41] As more S is loaded and utilized, meaning that more Li ions will be dissolved from and deposited to the Li electrode during cycling, the stability of the Li electrode becomes more important for good cycling stability of the cells.

In the comparison of the voltage profiles between the ionic liquid-containing electrolyte cell and the conventional electrolyte cell, the ionic liquid-containing cell showed a little larger discharge and charge overpotential and a smaller specific capacity at 0.2 mA/cm^2, which can be attributed to the higher Li ion mass transport resistance of the ionic liquid-containing electrolyte due to the high viscosity of the ionic liquid, according to the EIS results shown in Figure S13. Although the initial specific capacity of the ionic liquid-containing electrolyte cell (1200 mAh/gS) is smaller than that of the conventional electrolyte cell (1357 mAh/gS), the cycling stability of the ionic liquid-containing electrolyte cell is slightly better during 11 cycles than that of the conventional electrolyte cell. Especially, the excellent average Coulombic efficiency of 99.3 % (except the first cycle efficiency) was achieved, whereas the conventional electrolyte cell

showed the average Coulombic efficiency of only 95.7 %, which may be caused by the polysulfides dissolution into the electrolyte and their shuttle.

It was reported that the ionic liquid could prevent dendrite formation during cycling by forming a solid–electrolyte interphase (SEI) layer in symmetric Li/Li cells and the Li/$LiFEPO_4$ cell.[41] So it is worthwhile to verify, if the ionic liquid can help to stabilize the Li electrode in the high S loading cell. Surprisingly, the smooth surface of the pristine Li electrode (Figure 5c) became extremely irregular (Figure 5e), when it was cycled with conventional electrolyte. However, the morphology of the cycled Li electrode was much smoother with the ionic liquid-containing electrolyte (Figure 5d). This is a very important benefit, since hampering Li dendrite formation and growth on the Li electrode during cycling is one of the key challenges for a practical Li metal electrode based rechargeable cell in order to avoid cell shorting. Consequently, it may be important to employ a certain amount of ionic liquid in the electrolyte to stabilize the electrochemical behavior of the cell without sacrificing specific energy.

In summary, the S-GO-CTA-CNT nano-composite as a high performance cathode material for the Li/S cell was prepared and characterized. The real-time TEM observation results demonstrate that the nano-architecture of the S-GO-CTA-CNT composite results in the homogeneous formation of Li_2S nano-crystals and helps to maintain its structural integrity during lithiation. Further modification was made by the freeze drying method to enhance the exfoliation (separation) of the S-GO flakes. The cells with a high S loading of 2.3 ~ 11.5 mg/cm^2 and with reasonable S content of 64 ~ 75 % were developed using 3-D structured Al foam and especially the lowest E/S ratio of 4 was achieved with a high S loading electrode (11.1 mg/cm^2, 75 % S) without showing significant discharge overvoltage, while achieving a high specific capacity of

1128 mAh/gS (corresponding to 12.5 mAh/cm^2) at 0.2 mA/cm^2. Furthermore, the effect of the ionic liquid on the electrochemical behavior of the high S loading cell was demonstrated, which showed a higher Coulombic efficiency and a more stable Li electrode during cycling. We beileve that the achievements reported here will brighten the prospects for practical Li/S cells.

Methods

Synthesis of S-GO-CTA-CNT nano-composite

The S-GO-CTA-CNT nano-composite was prepared *via* a modified synthesis process from our previously-published method. Briefly, 0.58 g of sodium sulfide powder (Alfa Aesar, Na_2S, anhydrous) was dissolved in 25 mL of ultrapure water to form a Na_2S solution. A sample of 0.72 g of elemental sulfur powder (Alfa Aesar, S, ~ 325 mesh, 99.5 %) was added to the Na_2S solution and stirred with a magnetic stirrer at 60 °C until the solution became a transparent orange color (a sodium polysulfide (Na_2S_x) solution). 18 mL of single layer graphene oxide dispersion (GO, ACS materials, 10 mg/mL) in water was diluted to form a GO suspension (180 mg of GO in 180 mL of ultrapure water). 2.5 mmols of cetyltrimethyl ammonium bromide (164 mg, Sigma Aldrich, CTAB) was added to the GO suspension and stirred for 2 h with a magnetic stirrer. Then the prepared Na_2S_x solution was added to the GO-CTAB composite solution and stirred overnight. The as-prepared Na_2S_x–GO-CTAB composite solution was slowly added to 100 mL of 2.0 M formic acid (Aqua Solutions). During the acidification process, 20 mg of carbon nanotubes (CNT, OCSiAl) was dispersed in 10 ml water (2 mg/ml) using an ultra-sonicator with the assistance of 0.5 wt.% triton X-100 (Sigma). Two hours after the completion of the acidification reaction, the CNT dispersion was added into the acidified Na_2S_x–GO-CTAB

composite solution and stirred for an additional 1 hour. Finally, the S-GO-CTA-CNT nano-composite was filtered and washed with acetone and ultrapure water several times to remove salts and impurities. The obtained powder sample was dried at 50 °C in a vacuum oven overnight. The dried powder sample was ground using a mortar and pestle and heat-treated in a tube furnace at 155 °C for 12 h under an Ar atmosphere. For freeze drying, the synthesized S-GO-CTA-CNT nano-composite was filtered and washed with ultrapure water until the pH of the solution reached 7. Then the S-GO-CTA-CNT nano-composite suspension in approximately 100 ml of water was frozen at -85 ºC and lyophilized (Labconco) at 15 moor. The lyophilized powder sample was heat-treated in a tube furnace at 155 °C for 12 h under an Ar atmosphere.

Material characterization

The morphology of the powdered samples was observed using a scanning electron microscope (SEM, ZEISS Gemini Ultra 55) at an accelerating voltage of 5 kV. TEM observation with EDS mapping for elemental analyses was carried out with Genesis series (EDAX) equipped in Tecnai G2 F30S TEM (300 kV, FEI). For a 2D map, the dwell time on each pixel was set to 500 μs. Thermogravimetric analysis (TGA, TA Instruments Q5000) was used to determine the content of S in the S-GO-CTA-CNT nano-composite up to 600 ºC under a nitrogen atmosphere. X-ray photoelectron spectroscopy (XPS) was carried out to verify the chemical structures of the S-GO-CTA-CNT and S-GO-CNT nano-composites using a monochromatized Al Kα X-ray source (Quantum2000, Physical electronics, Chanhassen, MN, USA). The XPS spectra were deconvoluted by Gaussian curve fitting.

For SEM observation of the Li electrodes, the Li foil was gently scrubbed using a brush and rolled to get rid of impurities on the Li metal surface. For the ex-situ analyses, the Li metal electrodes were coupled with the S-GO-CTA-CNT electrodes in coin cells with an electrolyte composed of 1M LiTFSI in $PYR_{14}TFSI$/DOL/DME (1:1:1, *v/v*) with 0.5 M $LiNO_3$ or 1 M LiTFSI in DOL/DME (1:1:1, *v/v*) with 0.5 M $LiNO_3$ and cycled for 1 cycle. At the fully charged state, the cells were disassembled and the Li electrodes were collected. The collected Li metal electrodes were rinsed using a mixed solvent (DOL:DME=1:1, *v/v*) and dried. All processes were conducted in an Ar-filled glovebox.

***In situ* TEM observation**

With a gas mixture of methane (CH_4, 50 sccm) and hydrogen (H_2, 200 sccm) at 1050°C, large-area monolayer graphene was synthesized by chemical vapor deposition (CVD) on Cu foil (0.025 mm thick, Alfa Aesar). Then, it was directly transferred onto the two TEM grids (Quantifoil, 2/2, Au 300 Mesh). 0.5 mg of S-GO-CTA-CNT powder was mixed with 3 mL of 1M LiTFSI in a DOL/DME mixture solution (1:1 *v/v*). The mixture was dropped onto two graphene-coated TEM grids facing the graphene-side of each other using the same procedures as for the previous studies.[36] Before thorough drying of the excess EL solution, two TEM grids were separated and kept on a filtration paper for more than 10 hours. The GLC assembly process was conducted in an Ar-filled glove box system controlling the concentration of oxygen and moisture to less than 1 ppm to minimize the degradation of EL solution. The sample was loaded into the TEM column with minimum exposure to air. The unavoidable exposure time was less than a few seconds.

A field emission transmission electron microscope (TEM, Tecnai G2 F30, FEI) was used for monitoring the lithiation process in real time. In the scanning TEM mode, the electron beam dose rate were maintained to 22.5 – 25.0 $e^-/Å^2s$ and the dwell time on each pixel was set to 1 μs, as the minimum range to initiate the chemical lithiation but prevent electron beam-induced artifacts under 300 kV electron beam condition.

Electrochemical Tests

The S-GO-CTA-CNT electrode (64% S) was prepared by mixing the S-GO-CTA-CNT nano-composite, the mixture of CNT and Ketjenblack (KB, AkzoNobel, 1:1 *w/w*) as carbon additives and the styrene-butadiene rubber/carboxymethylcellulose (SBR/CMC, 8%, 1:1 *w/w*) composite binder at a weight ratio of 73.6:18.4:8 in water. The slurry was stirred using a magnetic stirrer overnight and cast onto the Al foam. For 70 %S and 75 %S electrodes, the compositions of the slurries were adjusted to 80.5:14.5:5 and 87.2:7.8:5, respectively, and the SBR binder with N-Methyl-2-pyrrolidone (NMP, Alfa Aesar) as solvent were used. For the comparisons, the same slurry (70 %S) was cast onto an Al foil current collector. Two different electrolytes composed of 1 M Lithium Bis(Trifluoromethanesulfonyl)Imide (Sigma Aldrich, LiTFSI) and 0.5 M $LiNO_3$ in N-methyl-N-butylpyrrolidinium bis(trifluoromethane sulfonyl)imide (Boulder Ionics, PYR_{14}TFSI)/1,3-dioxolane (Sigma Aldrich, DOL)/1,2-dimethoxyethane (Sigma Aldrich, DME) (2:1:1, *v/v*) and 1 M LiTFSI and 0.5 M $LiNO_3$ in DOL/DME (1:1, *v/v*) were used. 2032-type coin cells were fabricated with a lithium metal foil as counter/reference electrode and a porous polypropylene separator (2400, Celgard) in a glove box filled with Ar gas. Galvanostatic cycling tests of the coin cells were performed using a battery cycler (Maccor) at a given current density.

The electrochemical impedance was measured from 10 mHz to 1 MHz using a potentiostat (Biologic VSP) at the charged state.

FIGURES

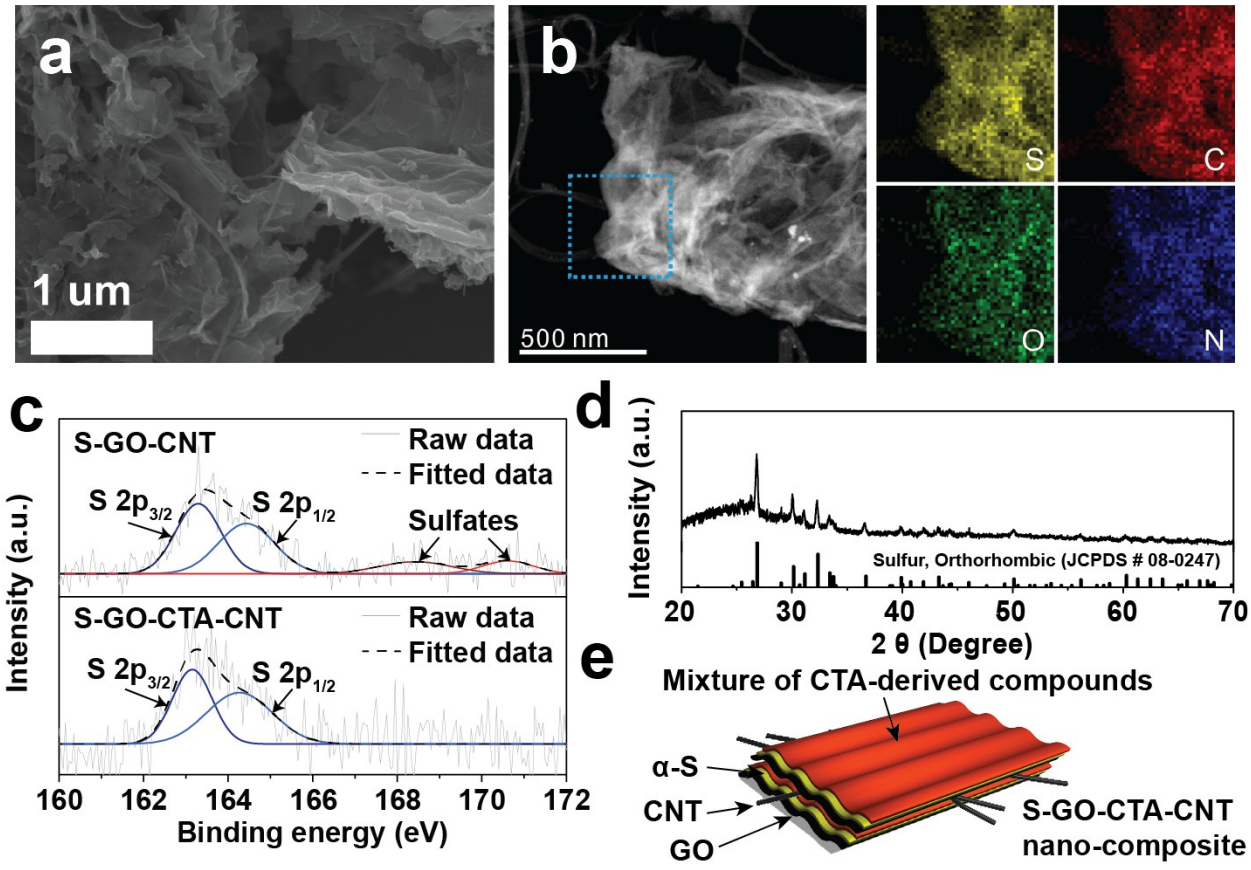

Figure 1. (a) SEM image and (b) TEM image with EDS elemental mapping results of the S-GO-CTA-CNT nano-composites. (c) XPS spectra of the S-GO-CNT and the S-GO-CTA-CNT nano-composites. (d) XRD pattern (cobalt-Kα) and (e) schematic illustration of the S-GO-CTA-CNT nano-composite.

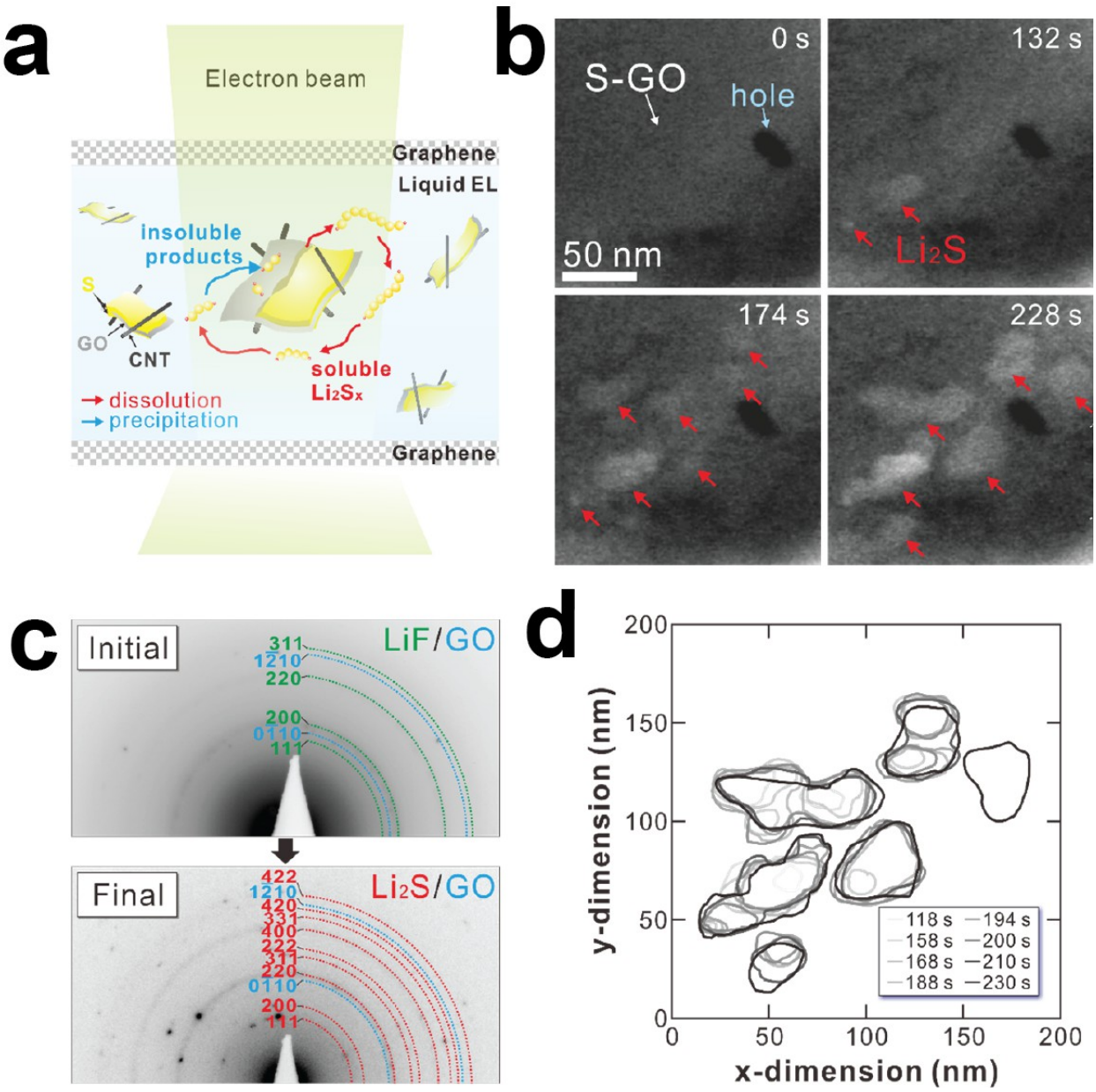

Figure 2. Lithiation processes of the S-GO-CTA-CNT nano-composite. (a) A schematic illustration of *in situ* GLC-TEM technique. (b) Time-series STEM images (Red arrows: Li_2S crystals; blue arrow: a hole.). (c) SA-EDPs at initial and final lithiation stages. (d) A graphical display of Li_2S crystals formation and growth (light gray: 118 s to black: 230 s) observed in Movie S1.

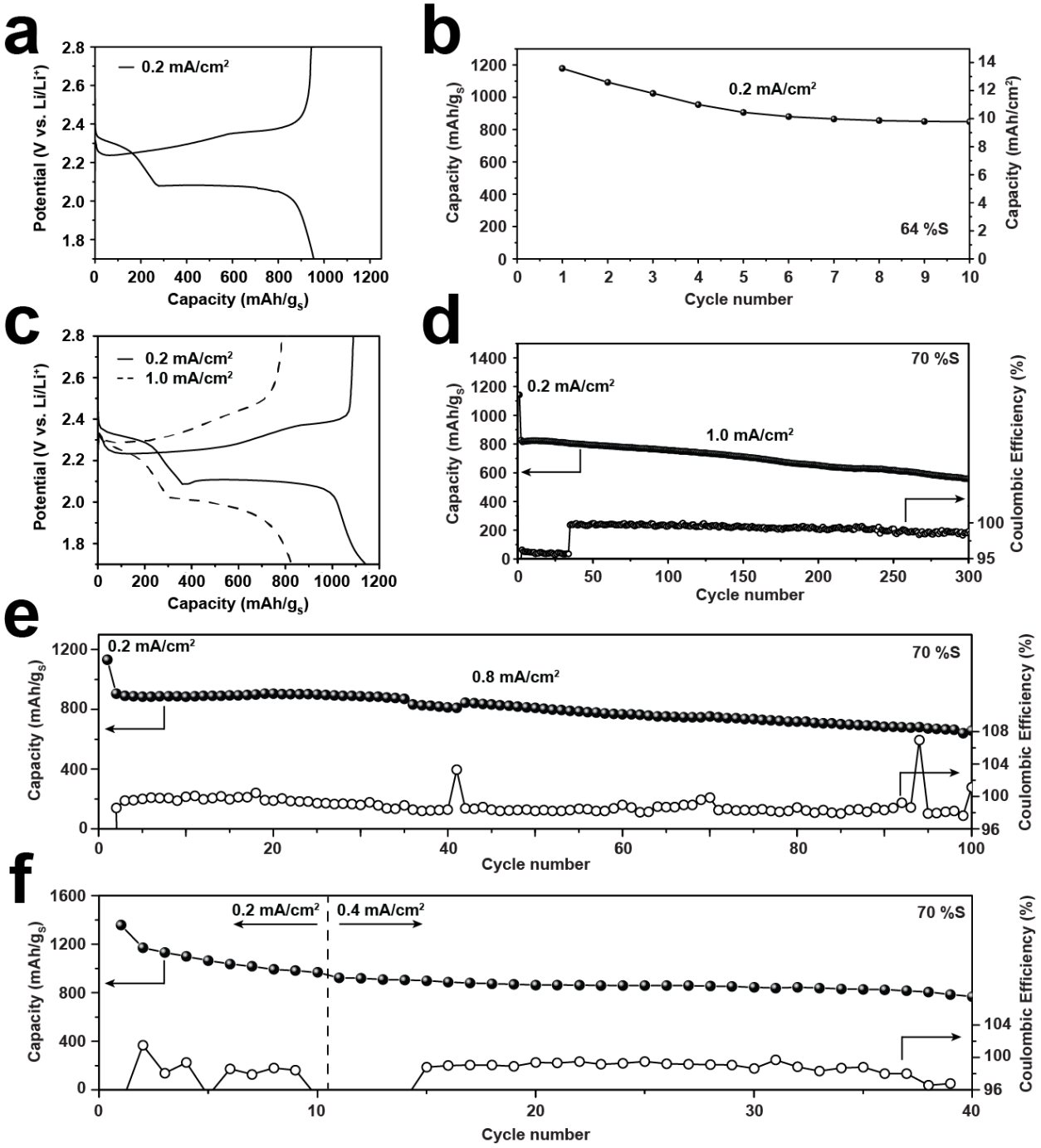

Figure 3. (a) Voltage profiles and (b) cycling performances of the S-GO-CTA-CNT electrode (S loading: 11.5 mg/cm^2, S content: 64 %, E/S ratio: 8). (c) Voltage profiles and (d) cycling performance of the S-GO-CTA-CNT electrode (S loading: 2.3 mg/cm^2, S content: 70 %, E/S

ratio: 45). (e) Cycling performance of the S-GO-CTA-CNT electrode (S loading: 4.2 mg/cm^2, S content: 70 %, E/S ratio: 10). The electrolyte composed of 1 M LiTFSI in PYR_{14}TFSI/DOL/DME (1:1:1, *v/v*) with 0.5 M $LiNO_3$ was used for the tests. (f) Cycling performance of the S-GO-CTA-CNT electrode (S loading: 7.9 mg/cm^2, S content: 70 %, E/S ratio: 7). The electrolyte composed of 1 M LiTFSI in PYR_{14}TFSI/DOL/DME (1:2:2, *v/v*) with 0.5 M $LiNO_3$ was used for the tests.

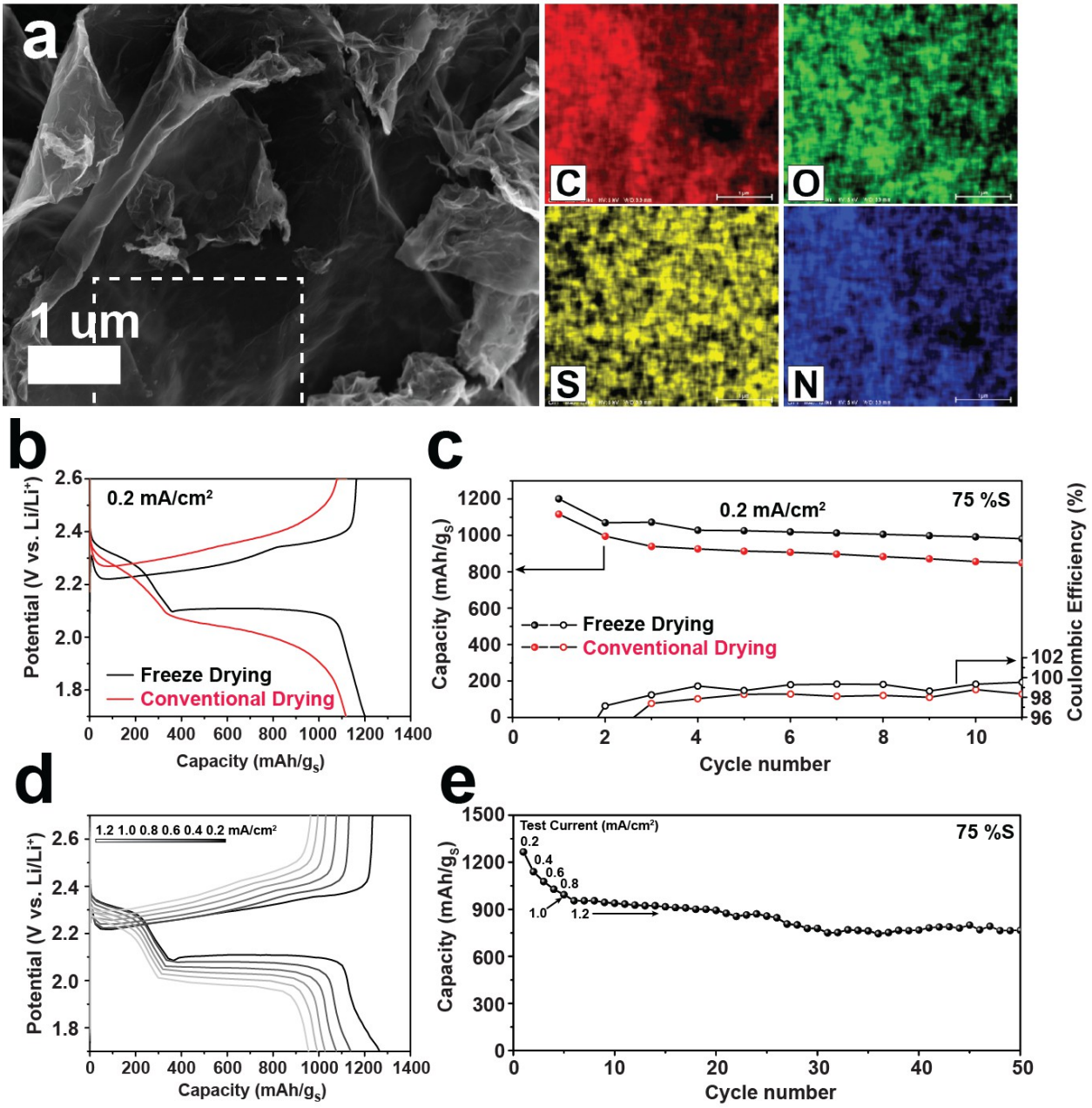

Figure 4. (a) SEM image with EDS elemental mapping results of the S-GO-CTA-CNT (FD) nano-composite. Comparisons of (b) voltage profiles and (c) cycling performances of the S-GO-CTA-CNT (FD) and the S-GO-CTA-CNT electrodes. Electrolyte composed of 1 M LiTFSI in $PYR_{14}TFSI$/DOL/DME (1:1:1, *v/v*) with 0.5 M $LiNO_3$ was used for the tests (E/S ratio: 10). Average S loading of the electrode was ~ 6.3 mg/cm^2. (d) Voltage profiles and (e) cycling

performances of the S-GO-CTA-CNT (FD) electrodes with the E/S ratio of 5. Electrolyte composed of 1 M LiTFSI in DOL/DME (1:1, *v/v*) with 0.5 M $LiNO_3$ was used for the tests. Average S loading of the electrodes was ~ 4.8 mg/cm^2.

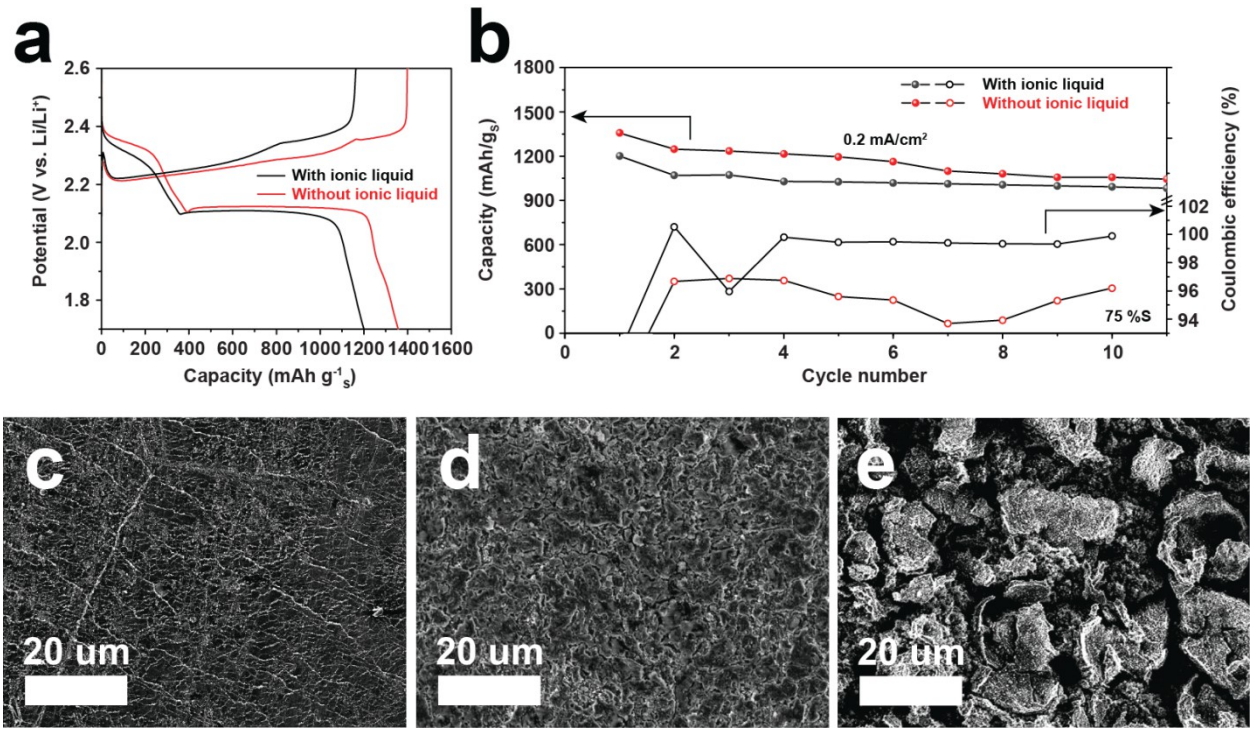

Figure 5. Comparisons of (a) voltage profiles and (b) cycling performances of the S-GO-CTA-CNT (FD) electrodes with the conventional electrolyte and the ionic liquid-containing electrolyte. The electrolytes were composed of 1 M LiTFSI in PYR_{14}TFSI/DOL/DME (1:1:1, *v/v*) with 0.5 M $LiNO_3$ or 1 M LiTFSI in DOL/DME (1:1, *v/v*) with 0.5 M $LiNO_3$. (E/S ratio: 10, average S loading: 6.3 mg/cm^2). SEM images of the Li electrodes. (c) Pristine, (d) cycled with the ionic liquid-containing electrolyte and (e) cycled with the conventional electrolyte.

ASSOCIATED CONTENT

Supporting Information.

Additional experimental results (PDF)

Movie showing the result of real-time TEM observation (AVI)

Corresponding Author

*Elton J. Cairns, Email: ejcairns@lbl.gov

Author Contributions

Elton J. Cairns planned the project and supervised the research conducted by Yoon Hwa in all aspects. Yoon Hwa designed the project details, performed design calculation and the experiments and co-authored the manuscript. Hyeon Kook Seo conducted TEM analyses and assisted in writing the manuscript. Jong-min Yuk designed in-situ TEM analysis and supervised the experiment conducted by Hyeon Kook Seo. All authors have given approval to the final version of the manuscript.

ACKNOWLEDGMENT

The work at LBNL was sponsored by ZAF Energy Systems. We thank Tevye Kuykendall and the Molecular Foundry at the Lawrence Berkeley National Laboratory for supporting the X-ray diffractometer, X-ray photoelectron spectroscopy and scanning electron microscope. Work at the Molecular Foundry was supported by the Office of Science, Office of Basic Energy Sciences, of the U.S. Department of Energy under Contract No. DE-AC02-05CH11231. The TEM research was supported by Nano•Material Technology Development Program through the National Research Foundation of Korea(NRF) funded by the Ministry of Science, ICT and Future

Planning.(2009-0082580). Dr. Hyo Won Kim and Hilda Buss are thanked for assistance with XPS analysis and freeze drying, respectively.

REFERENCES

1. Mikhaylik, Y. V.; Akridge, J. R., Polysulfide Shuttle Study in the Li/S Battery System. *J. Electrochem. Soc.* **2004,** *151* (11), A1969-A1976.
2. Ji, X.; Lee, K. T.; Nazar, L. F., A highly ordered nanostructured carbon-sulphur cathode for lithium-sulphur batteries. *Nat Mater* **2009,** *8* (6), 500-506.
3. Song, M.-K.; Zhang, Y.; Cairns, E. J., A Long-Life, High-Rate Lithium/Sulfur Cell: A Multifaceted Approach to Enhancing Cell Performance. *Nano Letters* **2013,** *13* (12), 5891-5899.
4. Wang, H.; Yang, Y.; Liang, Y.; Robinson, J. T.; Li, Y.; Jackson, A.; Cui, Y.; Dai, H., Graphene-Wrapped Sulfur Particles as a Rechargeable Lithium–Sulfur Battery Cathode Material with High Capacity and Cycling Stability. *Nano Letters* **2011,** *11* (7), 2644-2647.
5. Chen, R.; Zhao, T.; Lu, J.; Wu, F.; Li, L.; Chen, J.; Tan, G.; Ye, Y.; Amine, K., Graphene-Based Three-Dimensional Hierarchical Sandwich-type Architecture for High-Performance Li/S Batteries. *Nano Letters* **2013,** *13* (10), 4642-4649.
6. Tang, C.; Zhang, Q.; Zhao, M.-Q.; Huang, J.-Q.; Cheng, X.-B.; Tian, G.-L.; Peng, H.-J.; Wei, F., Nitrogen-Doped Aligned Carbon Nanotube/Graphene Sandwiches: Facile Catalytic Growth on Bifunctional Natural Catalysts and Their Applications as Scaffolds for High-Rate Lithium-Sulfur Batteries. *Advanced Materials* **2014,** *26* (35), 6100-6105.
7. Hwa, Y.; Zhao, J.; Cairns, E. J., Lithium Sulfide (Li2S)/Graphene Oxide Nanospheres with Conformal Carbon Coating as a High-Rate, Long-Life Cathode for Li/S Cells. *Nano Letters* **2015,** *15* (5), 3479-3486.
8. Guo, J.; Yang, Z.; Yu, Y.; Abruña, H. D.; Archer, L. A., Lithium–Sulfur Battery Cathode Enabled by Lithium–Nitrile Interaction. *Journal of the American Chemical Society* **2013,** *135* (2), 763-767.
9. Moon, S.; Jung, Y. H.; Jung, W. K.; Jung, D. S.; Choi, J. W.; Kim, D. K., Encapsulated Monoclinic Sulfur for Stable Cycling of Li–S Rechargeable Batteries. *Advanced Materials* **2013,** *25* (45), 6547-6553.
10. Tao, X.; Wang, J.; Ying, Z.; Cai, Q.; Zheng, G.; Gan, Y.; Huang, H.; Xia, Y.; Liang, C.; Zhang, W.; Cui, Y., Strong Sulfur Binding with Conducting Magnéli-Phase TinO2n–1 Nanomaterials for Improving Lithium–Sulfur Batteries. *Nano Letters* **2014,** *14* (9), 5288-5294.
11. Liang, X.; Hart, C.; Pang, Q.; Garsuch, A.; Weiss, T.; Nazar, L. F., A highly efficient polysulfide mediator for lithium–sulfur batteries. *Nature Communications* **2015,** *6*, 5682.
12. Ji, X.; Evers, S.; Black, R.; Nazar, L. F., Stabilizing lithium–sulphur cathodes using polysulphide reservoirs. *Nature Communications* **2011,** *2*, 325.
13. Chen, Y.; Lu, S.; Wu, X.; Liu, J., Flexible Carbon Nanotube–Graphene/Sulfur Composite Film: Free-Standing Cathode for High-Performance Lithium/Sulfur Batteries. *The Journal of Physical Chemistry C* **2015,** *119* (19), 10288-10294.

14. Chen, Y.; Lu, S.; Zhou, J.; Qin, W.; Wu, X., Synergistically Assembled Li2S/FWNTs@Reduced Graphene Oxide Nanobundle Forest for Free-Standing High-Performance Li2S Cathodes. *Advanced Functional Materials* **2017,** *27* (25), n/a-n/a.
15. Hagen, M.; Fanz, P.; Tübke, J., Cell energy density and electrolyte/sulfur ratio in Li–S cells. *Journal of Power Sources* **2014,** *264*, 30-34.
16. Kim, H. M.; Sun, H.-H.; Belharouak, I.; Manthiram, A.; Sun, Y.-K., An Alternative Approach to Enhance the Performance of High Sulfur-Loading Electrodes for Li–S Batteries. *ACS Energy Letters* **2016,** *1* (1), 136-141.
17. Qie, L.; Manthiram, A., High-Energy-Density Lithium–Sulfur Batteries Based on Blade-Cast Pure Sulfur Electrodes. *ACS Energy Letters* **2016,** *1* (1), 46-51.
18. Li, Z.; Zhang, J. T.; Chen, Y. M.; Li, J.; Lou, X. W., Pie-like electrode design for high-energy density lithium–sulfur batteries. *Nature Communications* **2015,** *6*, 8850.
19. Hu, G.; Xu, C.; Sun, Z.; Wang, S.; Cheng, H.-M.; Li, F.; Ren, W., 3D Graphene-Foam–Reduced-Graphene-Oxide Hybrid Nested Hierarchical Networks for High-Performance Li–S Batteries. *Advanced Materials* **2016,** *28* (8), 1603-1609.
20. Fang, R.; Zhao, S.; Hou, P.; Cheng, M.; Wang, S.; Cheng, H.-M.; Liu, C.; Li, F., 3D Interconnected Electrode Materials with Ultrahigh Areal Sulfur Loading for Li–S Batteries. *Advanced Materials* **2016,** *28* (17), 3374-3382.
21. Qie, L.; Manthiram, A., A Facile Layer-by-Layer Approach for High-Areal-Capacity Sulfur Cathodes. *Advanced Materials* **2015,** *27* (10), 1694-1700.
22. Zhou, G.; Li, L.; Ma, C.; Wang, S.; Shi, Y.; Koratkar, N.; Ren, W.; Li, F.; Cheng, H.-M., A graphene foam electrode with high sulfur loading for flexible and high energy Li-S batteries. *Nano Energy* **2015,** *11*, 356-365.
23. Hagen, M.; Dörfler, S.; Althues, H.; Tübke, J.; Hoffmann, M. J.; Kaskel, S.; Pinkwart, K., Lithium–sulphur batteries – binder free carbon nanotubes electrode examined with various electrolytes. *Journal of Power Sources* **2012,** *213*, 239-248.
24. Cheng, X.-B.; Peng, H.-J.; Huang, J.-Q.; Zhu, L.; Yang, S.-H.; Liu, Y.; Zhang, H.-W.; Zhu, W.; Wei, F.; Zhang, Q., Three-dimensional aluminum foam/carbon nanotube scaffolds as long- and short-range electron pathways with improved sulfur loading for high energy density lithium–sulfur batteries. *Journal of Power Sources* **2014,** *261*, 264-270.
25. Miao, L.; Wang, W.; Yuan, K.; Yang, Y.; Wang, A., A lithium-sulfur cathode with high sulfur loading and high capacity per area: a binder-free carbon fiber cloth-sulfur material. *Chemical Communications* **2014,** *50* (87), 13231-13234.
26. Yu, M.; Ma, J.; Xie, M.; Song, H.; Tian, F.; Xu, S.; Zhou, Y.; Li, B.; Wu, D.; Qiu, H.; Wang, R., Freestanding and Sandwich-Structured Electrode Material with High Areal Mass Loading for Long-Life Lithium–Sulfur Batteries. *Advanced Energy Materials* **2017,** *7* (11), n/a-n/a.
27. Hong, X.; Jin, J.; Wu, T.; Lu, Y.; Zhang, S.; Chen, C.; Wen, Z., A rGO-CNT aerogel covalently bonded with a nitrogen-rich polymer as a polysulfide adsorptive cathode for high sulfur loading lithium sulfur batteries. *Journal of Materials Chemistry A* **2017,** *5* (28), 14775-14782.

28. Qin, F.; Wang, X.; Zhang, K.; Fang, J.; Li, J.; Lai, Y., High areal capacity cathode and electrolyte reservoir render practical Li-S batteries. *Nano Energy* **2017,** *38*, 137-146.
29. Li, M.; Carter, R.; Douglas, A.; Oakes, L.; Pint, C. L., Sulfur Vapor-Infiltrated 3D Carbon Nanotube Foam for Binder-Free High Areal Capacity Lithium–Sulfur Battery Composite Cathodes. *ACS Nano* **2017,** *11* (5), 4877-4884.
30. Quan, B.; Yu, S.-H.; Chung, D. Y.; Jin, A.; Park, J. H.; Sung, Y.-E.; Piao, Y., Single Source Precursor-based Solvothermal Synthesis of Heteroatom-doped Graphene and Its Energy Storage and Conversion Applications. *Scientific Reports* **2014,** *4*, 5639.
31. Schaufuß, A. G.; Nesbitt, H. W.; Kartio, I.; Laajalehto, K.; Bancroft, G. M.; Szargan, R., Incipient oxidation of fractured pyrite surfaces in air. *Journal of Electron Spectroscopy and Related Phenomena* **1998,** *96* (1–3), 69-82.
32. Kim, H.; Lee, J. T.; Magasinski, A.; Zhao, K.; Liu, Y.; Yushin, G., In Situ TEM Observation of Electrochemical Lithiation of Sulfur Confined within Inner Cylindrical Pores of Carbon Nanotubes. *Advanced Energy Materials* **2015,** *5* (24), n/a-n/a.
33. Yang, Z.; Zhu, Z.; Ma, J.; Xiao, D.; Kui, X.; Yao, Y.; Yu, R.; Wei, X.; Gu, L.; Hu, Y.-S.; Li, H.; Zhang, X., Phase Separation of Li2S/S at Nanoscale during Electrochemical Lithiation of the Solid-State Lithium–Sulfur Battery Using In Situ TEM. *Advanced Energy Materials* **2016,** *6* (20), n/a-n/a.
34. Xu, Z.-L.; Huang, J.-Q.; Chong, W. G.; Qin, X.; Wang, X.; Zhou, L.; Kim, J.-K., In Situ TEM Study of Volume Expansion in Porous Carbon Nanofiber/Sulfur Cathodes with Exceptional High-Rate Performance. *Advanced Energy Materials* **2017**, n/a-n/a.
35. Yuk, J. M.; Park, J.; Ercius, P.; Kim, K.; Hellebusch, D. J.; Crommie, M. F.; Lee, J. Y.; Zettl, A.; Alivisatos, A. P., High-Resolution EM of Colloidal Nanocrystal Growth Using Graphene Liquid Cells. *Science* **2012,** *336* (6077), 61-64.
36. Yuk, J. M.; Seo, H. K.; Choi, J. W.; Lee, J. Y., Anisotropic Lithiation Onset in Silicon Nanoparticle Anode Revealed by in Situ Graphene Liquid Cell Electron Microscopy. *ACS Nano* **2014,** *8* (7), 7478-7485.
37. Cheong, J. Y.; Chang, J. H.; Seo, H. K.; Yuk, J. M.; Shin, J. W.; Lee, J. Y.; Kim, I.-D., Growth dynamics of solid electrolyte interphase layer on SnO2 nanotubes realized by graphene liquid cell electron microscopy. *Nano Energy* **2016,** *25*, 154-160.
38. Lang, S.-Y.; Shi, Y.; Guo, Y.-G.; Wang, D.; Wen, R.; Wan, L.-J., Insight into the Interfacial Process and Mechanism in Lithium–Sulfur Batteries: An In Situ AFM Study. *Angewandte Chemie International Edition* **2016,** *55* (51), 15835-15839.
39. Park, J.-W.; Ueno, K.; Tachikawa, N.; Dokko, K.; Watanabe, M., Ionic Liquid Electrolytes for Lithium–Sulfur Batteries. *The Journal of Physical Chemistry C* **2013,** *117* (40), 20531-20541.
40. Wang, L.; Liu, J.; Yuan, S.; Wang, Y.; Xia, Y., To mitigate self-discharge of lithium-sulfur batteries by optimizing ionic liquid electrolytes. *Energy & Environmental Science* **2016,** *9* (1), 224-231.
41. Basile, A.; Bhatt, A. I.; O'Mullane, A. P., Stabilizing lithium metal using ionic liquids for long-lived batteries. *Nature Communications* **2016,** *7*, ncomms11794.